Journal of Cleaner Production 380 (2022) 134947

Contents lists available at ScienceDirect

Journal of Cleaner Production

journal homepage: www.elsevier.com/locate/jclepro

The importance of the functional mixed entropy for the explanation of residential and transport CO_2 emissions in the urban center of China

Shudi Zuo [a,b,*], Shaoqing Dai [c], Jiaheng Ju [a,b], Fanxin Meng [d], Yin Ren [a], Yunfeng Tian [a,b], Kaide Wang [e]

[a] Key Laboratory of Urban Environment and Health, Fujian Key Laboratory of Watershed Ecology, Key Laboratory of Urban Metabolism of Xiamen, Institute of Urban Environment, Chinese Academy of Sciences, Xiamen, 361021, China
[b] University of Chinese Academy of Sciences, Beijing, 100049, China
[c] Faculty of Geo-information Science and Earth Observation (ITC), University of Twente, Enschede, 7500 AE, the Netherlands
[d] State Key Joint Laboratory of Environment Simulation and Pollution Control, School of Environment, Beijing Normal University, Beijing, 100875, China
[e] Yunnan Ecological and Environmental Monitoring Center, Kunming, 650034, China

ARTICLE INFO

Handling Editor: Jing Meng

Keywords:
CO_2 mapping
Downscaling interpolation
Functional mixed entropy
Urban form
Spatial analysis

ABSTRACT

The influence of urban spatial form on the environment is complex and lengthy. The spatial analysis for the urban form and residential-related CO_2 emissions at the city scale is challenging due to the lack of extensive urban form data and fine-grain CO_2 emission maps. This research uses remote sensing data and downscaling interpolation to generate residential and transport (RTCE) maps in 130 m spatial resolution of urban center regions from 31 major cities in China, then investigates the relationship between 3 types of urban form indicators (Internal characteristics, external morphology, and development intensity) and RTCE through Geographical Weighted Regression method. The results reveal that urban form indicators could explain about 45.9% of RTCE. The 2D building shape indicator has the second greatest positive impact as the external morphology indicator, which complicates the influence. The internal characteristics indicators have relatively strong influences than the development intensity indicators. For instance, the influence of functional mixed entropy (FME) is the greatest positive influence and decreases exponentially with FME increases. Therefore, cities with the FME lower than the threshold (0.28) should increase it appropriately, while cities with the FME around and larger than 0.28 should maintain and probably reduce it.

1. Introduction

The 70%–80% of urban CO_2 emissions in developed countries are generated by household activity (housing and transportation). By 2050, urban residents will reach 66% of the global population (Larsson et al., 2019; Liu et al., 2021; United Nations, 2014). The emissions from residents' transportation choice & distance and residential energy consumption/use is proved to be influenced by urban form (Lee and Lee, 2014). Therefore, scholars are committed to adjusting urban form to reduce environmental impacts (e.g., low-carbon city). The urban form is a spatial system composed of the urban layout (the spatial location of various urban elements), urban morphology (the external contour and structure of the city), and interrelations (the interaction between urban elements) (Xia et al., 2017). The representative indicators are from the aspects of external morphology, internal element spatial form, development intensity, and so on (Sharifi, 2019). Urban morphology from an historico-geographical perspective, records the physical element changes and studies the agents and processes shaping the transformation of urban form over time (Oliveira, 2019). With the process of urbanization, the profound impact of urban form on CO2 emissions is inevitable. Although different city types follow different evolution paths, similar urban form may lead to similar spatial characteristics of residential and transport CO2 emissions (RTCE). Based on this premise, defining multiple urban forms and understanding the relationship between typical urban forms and RTCE patterns could serve as a basis for inferring emission trends and guide practical management (Sharifi et al., 2018).

However, it is exceptionally challenging to curb the growth of CO2

* Corresponding author. Key Laboratory of Urban Environment and Health, Fujian Key Laboratory of Watershed Ecology, Key Laboratory of Urban Metabolism of Xiamen, Institute of Urban Environment, Chinese Academy of Sciences, Xiamen, 361021, China.
E-mail address: sdzuo@iue.ac.cn (S. Zuo).

https://doi.org/10.1016/j.jclepro.2022.134947
Received 8 April 2022; Received in revised form 23 October 2022; Accepted 28 October 2022
Available online 2 November 2022

emissions through urban form adjustment. Firstly, the previous research about the relationship between urban CO_2 emissions and morphological characteristics focused on one or more of the building, community, or neighborhood scale. As the accounting system gradually improved, a series of urban, regional, or national scale research appeared. However, the accounting unit's total or the average CO2 emissions were used in the panel or time series analysis. The spatial heterogeneity of urban CO2 emission distribution caused by the composition and configuration of different urban functional areas cannot be captured (Knappe et al., 2022; Liu et al., 2015). Secondly, the diversity of urban form indicators resulted in the inconsistency and incomparability of the studies (Zhang et al., 2021). Urban form indicators reflect the characteristics at the building and block scales, including ratios of building surfaces, volumes or lengths, building density, porosity, and compacity, among others (Santos et al., 2021). Many studies have been carried out mainly on mediating impact factors, urban form characterization methods, quantification of actual impacts, and so on (Feyisa et al., 2014; Geng et al., 2017; Ye et al., 2015). The landscape metrics of each grid pixel were the simple quantitative indicators reflecting the characteristics of urban structure composition and spatial configuration. Nevertheless, the scale sensitivity problem would bring the results bias. Furthermore, due to the limitation of acquiring urban architectural data, a few studies represented the building in detail (Wu et al., 2018).

In addition, the mechanisms between urban form and RTCE are indirect and complex. The intermediary factors were different among cities. The time series and panel analysis showed that the urban sprawl of the mono-center city, fragmentation and random development had positive impacts on CO_2 emissions (Wang et al., 2015, 2018; S. Wang et al., 2018). Urban form influences RTCE by residential choice, travel characteristics, and surrounding thermal environment (Fan and Myint, 2014; Meng and Zacharias, 2021; Ou et al., 2013; Wang et al., 2015). Further studies showed that ignoring the spatial location, inherent geographical characteristics and urban characteristics of RTCE sources may lead to errors in research results (Wang et al., 2016). Moreover, internal differences of the urban form may lead to significant changes in CO2 emissions. Therefore, in order to understand the ideal urban pattern and discover the general effect rule of urban form on RTCE, it is necessary to bring the urban scale effect into consideration and break the limitation of administrative boundary on data, so as to explore the effect of the pattern of different urban functional areas on RTCE (Zuo et al., 2020).

This study aimed to establish an approach to investigate the relationship between urban form and RTCE in order to find practical guidance for the low-carbon city based on 31 Chinese major cities' experimental data. Eight indicators were established to quantify urban form. With these city-level data, the Geographically Weighted Regression was utilized to investigate the effects of urban form on RTCE, which was downscaled from the Global Carbon Grid v1.0 data. The study was not only to fill the gaps about the lack of spatial heterogeneous information and data at the pixel level but also to explore the influencing mechanism of internal characteristics, external morphology, and development intensity urban form indicators on RTCE.

2. Data and methodologies

2.1. Study region

31 developing Chinese cities were selected as study areas. Most of the 31 cities with the available urban form data were provincial capitals (Fig. 1). In the past 20 years, China has been experiencing rapid urbanization, accompanied by a large population aggregation, energy consumption, and CO2 emissions. China's total household CO_2 emissions accounted for 42.17% of the national CO_2 emissions, and household direct CO_2 emissions accounted for 27.55% of the total household CO_2 emissions (Liu et al., 2011). CO2 emissions from both rural and urban households are increasing. The highly urbanized urban center has

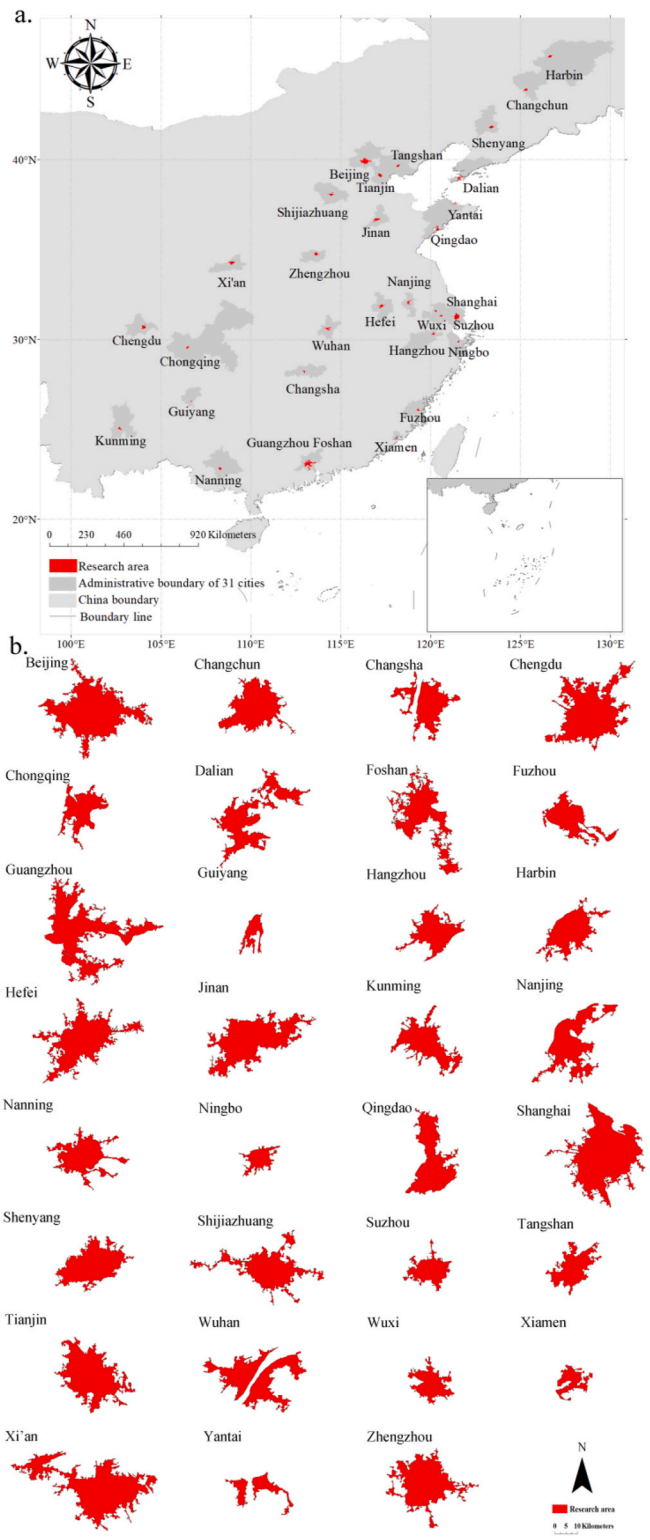

Fig. 1. The research areas of 31 cities.

mature administrative, commercial, and infrastructure facilities and is a typical region to study the impact of urban form on RTCE. According to Global Urban Boundary (GUB) dataset (Li et al., 2020), we defined the urban centers as the study areas that have been already urbanized since 2000. Compared with the existing urban center region, the scattered and fragmented regions, which might belong to the traditional town center, were eliminated. The city in this study refers to the city center region we identified. The analysis result of these cities could reveal the potential

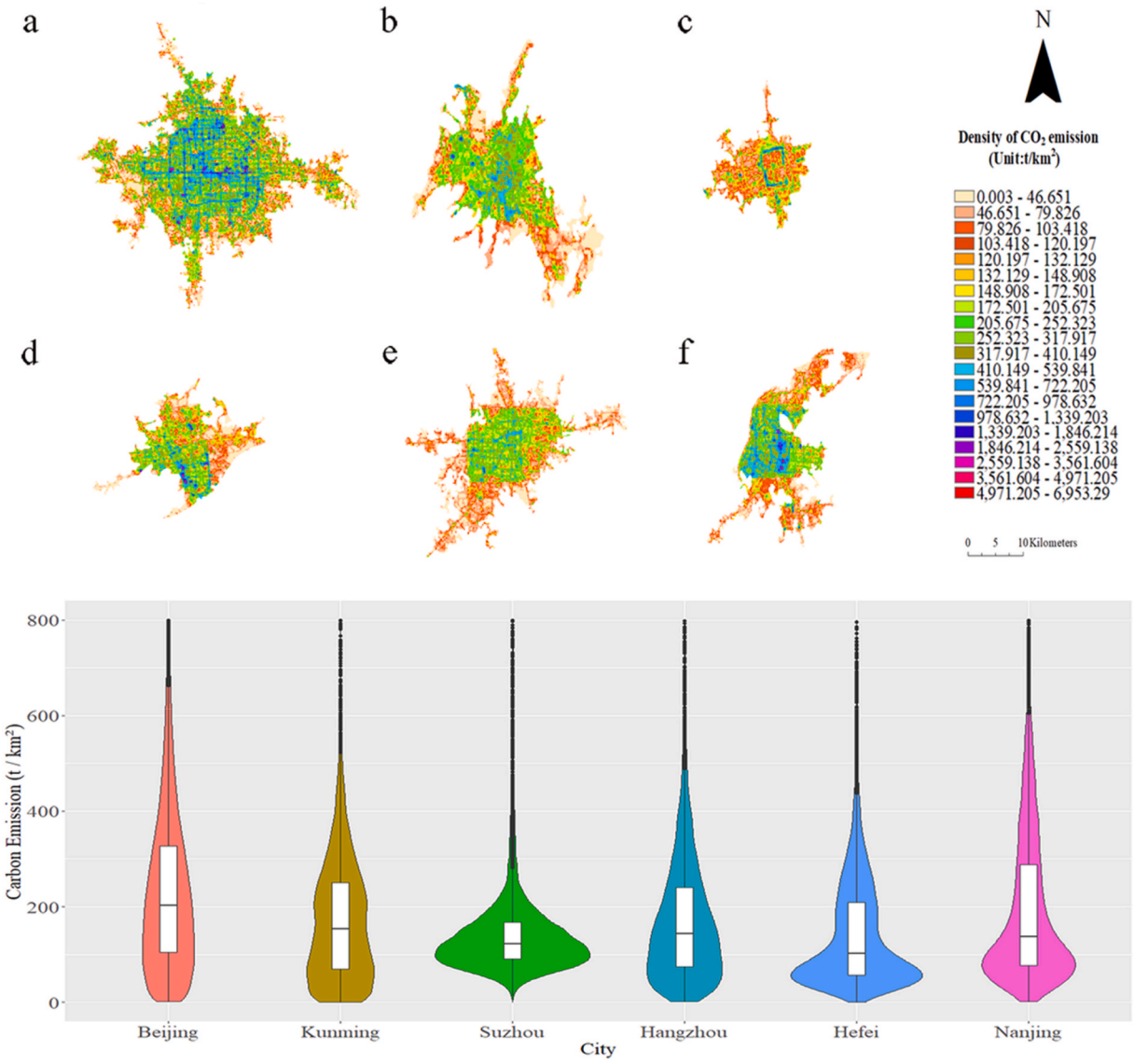

Fig. 2. Spatial pattern of residential CO_2 emission in a. Beijing (Type I—high green space and road length density), b. Kunming (Type II—high functional mixed entropy), c. Suzhou (Type III—similar but higher form indicator values than Type IV, except for green space density), d. Hangzhou (Type III), e. Hefei (Type IV), f. Nanjing (Type IV).

association between the urban form of urban center areas and RTCE in China.

2.2. Data sources

The original CO_2 emissions in this study were derived from the Global Carbon Grid v1.0 of Global Infrastructure Emission Database (GID) produced by Department of Earth System Science Tsinghua University.[1] The Global Carbon Grid v1.0 provides global 0.1° × 0.1°[2] energy consumption CO_2 emission map for six sectors in 2019, which includes power, industry, residential, transport, shipping, and aviation. Except for the point source data, residential sector data of GID are from International Energy Agency (IEA) and include the household consumption, excluding the fuel used for transport. The urban and rural population densities are used as the proxy to interpolate the CO_2 emissions. Transport sector data are from IEA CO_2 emission data and are interpolated and distributed onto road atlas (Meijer et al., 2018) based on the weights of the different types (Zheng et al., 2014). In terms of the IEA transport sector CO_2 emissions data,[3] the ratio of global emissions from the passenger road vehicles and road freight vehicles is about 3:2. The weights of the emissions from passenger road vehicles and freight trucks on the county road, which is the major road type in the urban center region, are 80% and around 15% (Zheng et al., 2014). Therefore, each grid value of GID transport emissions generally could be divided into 1 unit freight and 8 unit passenger emissions. Furthermore, there are restriction rules for the heavy and medium duty freight vehicles in the urban center regions in China due to the air pollution control. In brief, the freight vehicle's CO_2 emissions account for a small part of the emissions in the urban center region.

Since the spatial resolution of the GID data is coarse, we downscaled

[1] http://gidmodel.org.cn/.

[2] 0.1°is equal to approximately 11.1 km at the equator.

[3] IEA, Transport sector CO_2 emissions by mode in the Sustainable Development Scenario, 2000–2030, IEA, Paris.https://www.iea.org/data-and-statistics/charts/transport-sector-co2-emissions-by-mode-in-the-sustainable-development-scenario-2000-2030.

the CO_2 emissions using the Luojia 1-01 nighttime light imagery data[4] as the proxy variable, whose spatial resolution is about 130 m, to produce the more satisfactory resolution gridded CO_2 maps in order to meet the analysis requirement of the core urban region (Jiang et al., 2018). The nighttime light imagery of China was derived from 275 images of Luojia 1-01 captured from June to December 2018 and had less than 0.983 pixels median error in positioning accuracy. Based on the high-resolution image, we used the digital number (DN) values as the weight to allocate the Luojia grid CO_2 emissions.

We used eight indicators from the perspective of external morphology (e.g., building shape index (LSI) and building floor (BF)), internal characteristics (e.g., functional mixed entropy (FME), bus station density (BS), and road intersection density (RI)), and development intensity (e.g., road length density (RL), green space density (GS), and building area density (BA)) to depict the urban form in the study area. They were calculated based on data mainly including the Points of Interest (POI) data with spatial attribute information, building data, road network data, and essential urban land use categories (EULUC) data (Gong et al., 2020). Please see supplementary material for details.

2.3. Urban form description and classification

The urban layout directly impacts microclimate parameters (e.g., temperature), whose adjustment would bring additional energy consumption and CO_2 emissions. In terms of the building influences on land surface temperature modeling, the 3D indicators are more determinant than 2D ones (Santos et al., 2021). Therefore, building height and shape index were selected to represent the external morphology. Floors from building outline data represented building height. The shape index of landscape metrics was used to measure the deviation degree between the building shape and the circle of the same area. The large value represents the complexity of the patches or the proportion of the perimeter to the area of patches. This indicator is sensitive to the size of the patches. The calculation equation is as follows:

$$LSI_i = \frac{S_i}{2\sqrt{\pi A_i}} \tag{1}$$

where LSI_i is the building shape index on the grid i. S_i is the perimeter of the building, and A_i is the area of building patches on the grid i.

The internal characteristic indicator selection mainly depends on the intermediate factors of urban form influence. These indicators are related to building (size and type) and travel behavior (distance and type) (Ewing and Rong, 2008), which reveal the action path of the internal influence mechanisms and the common characteristics of different types of urban forms. Therefore, the BS, RI, and FME, which have impacts on the travel behavior, were selected as the internal characteristic indicators. BS (including the metro, bus, and BRT) were calculated through the zonal statistics tool in ArcMap 10.3 based on POI data. The RI was calculated through the feature vertices to points and spatial join functions in ArcMap 10.3 based on road network data. Frank and Pivo proposed an information entropy model based on different types of POI data according to the basic principle of information entropy (Pivo and Frank, 1994). The FME, which measures the mixing degree of functional areas, was based on the principle of information entropy calculation according to the point category of POIs. In this study, the POI dataset contains N (N = 11) categories, such as educational, industry, medical, hotel, residential, administrative, transportation facilities, blue & green space and tourist attraction, entertainment industry, catering trade, other commercial fields (Table A1). If each category includes T_1, T_2 … T_n, then $T = T_1+T_2+ \ldots\ldots +T_n = \Sigma_k T_k$ (k = 1, 2, …, n), and its probability can be defined as:

$$P_i = \frac{T_i}{T} = \frac{T_i}{\sum_i^N T_i} \tag{2}$$

$$H = -\sum_{i=1}^{N} P_i \times logP_i \tag{3}$$

where $\sum P_i = 1$, H ($H \geq 0$)is the information entropy representing the mixing degree of various urban functional types. The higher the H value is, the more diverse the land use functions are. When $T_1 = T_2 = \ldots\ldots = T_n$ and $P_1 = P_2 = \ldots\ldots = P_n = 1/N$, H reaches the maximum ($H_m = logN_\circ$). If $P_e = 1/N$, the mixing degree of the urban functional area has reached a stable state.

To calculate the information entropy of each raster grid, the formula is as follows:

$$P_{ij} = \frac{T_{ij}}{T_k} \tag{4}$$

$$H_s = -\sum_{i=1}^{M}\sum_{j=1}^{N} P_{ij} \times logP_{ij} \tag{5}$$

where $\sum_i\sum_j P_{ij} = 1$.H_s is the spatial information entropy of grid MN and the sum of information entropy of all different types of POIs in this grid. The higher the information entropy value is, the higher the mixing degree of the functional area is.

Development indicators represent the morphological characteristics brought by the urban scale effect and match with the development of economic activities. The GS, RL, and BA were selected as the development indicators. The GS was calculated through zonal statistics in ArcMap 10.3 based on the EULUC data. RL and BA were calculated by building outline data. The calculation formula is as follows:

$$R_d = \frac{L_{mn}}{S} \tag{6}$$

$$B_d = \frac{BA_{mn}}{S} \tag{7}$$

where R_d is road length density, B_d is building area density, L_{mn} is road length (m), BA_{mn} is building area (m^2) in the grid mn, and S is grid area (m^2).

Eight indicators of each grid in 31 cities were standardized through Min-Max normalization. In terms of the eight indicators, we classified 31 cities into 4 categories (TypeI, II, III, and IV) using the K-Means method (Figure A1 and A2). Please see supplementary material for details. K-Means method is a quick clustering method with low algorithm complexity and high efficiency (Molla et al., 2022). Differences among the clusters of urban form indicators were tested using the T-test by SPSS (Version 16.0) (Table A2). Then the mean values of each group were calculated.

2.4. RTCE map downscaling interpolation and anlysis

Since 31 cities are distributed in different regions of China, the GCS_WGS_1984 geographic coordinates of GID and Luojia 1-01 remote sensing images are projected into UTM Zone 48–52 coordinated system and WGS 1984 datum. The road intersections of each city were selected to match GID and Luojia data through the georeference tool in ArcMap 10.3. The 3–12 control points of the intersections were registered uniformly throughout the study region. We dropped the control points, which had the residual error larger than one gird resolution. After masking with the 31 study area boundaries, the downscaling interpolation was carried out.

The total CO_2 emissions in each small Luojia grid were calculated as follows (Fig. 2 for the typical cities of four different urban forms recognized via the K-means cluster map (Figure A2)).

[4] http://59.175.109.173:8888/app/login_en.html.

$$\begin{cases} C_i = \frac{DN_i}{DN_j} \times C_j \end{cases} \quad (8)$$

$$\begin{cases} DN_j = \sum_1^k DN_{i,1} + \ldots + DN_{i,k} \end{cases} \quad (9)$$

C_i is the CO_2 emissions of small Luojia 1-01 grid i. DN_i is the night light brightness of the Luojia grid i. DN_j is the night light brightness of GID rid j, and is the sum of all Luojia 1-01 grids in the 0.1° grid. C_j is the total CO_2 emission of GID grid j. The mean R^2 between the CO_2 and DN values of the Luojia data in 31 cities is 0.796 (Table A3).

Global Moran's I reflects the global spatial autocorrelation between different geographical regions and was used to analyze the spatial autocorrelation. Moran's I value is between −1 and 1, whereby the positive value indicates the similarity, while the negative value indicates the difference of the grids. The local Getis G_i^* was used to identify the cold (Low-Low cluster) and hot (High-High cluster) spots area of the RTCE maps.

2.5. Geographically Weighted Regression (GWR) method

The GWR method of Arcmap 10.3 was used to analyze the relationship between the urban form and RTCE due to the correlation and heterogeneity of the spatial data. The GWR model belongs to the Spatial Varying-Coefficient Regression model, expanded the linear regression model to make the regression coefficient b change with the spatial position of i. The coefficient reflects how the independent variables impact the dependent variables that change with spatial position. The equation is as follows.

$$y_i = \beta_0(u_i, v_i) + \sum_k \beta_k(u_i, v_i) x_{ik} + \varepsilon_i \quad i = 1, 2, \cdots, n \quad (10)$$

where y_i is the dependent variable at grid *i*, (u_i, v_i) is the location of grid *i*, $\beta_k(u_i, v_i)$ is the *k*th regression coefficient of grid *i*. The continuous function β_k is a function of distance attenuation, where the Gaussian kernel function is used, and the bandwidth is the feature scale. x_{ik} is the value of the k-th independent variable at grid i.ε_i is the residual. The coefficients of the independent variables represent the influence direction and power on RTCE. We used the variance inflation factor (VIF), equal to $1/(1\text{-}R^2)$, to measure the collinearity. *R* is the negative regression correlation coefficient of the other independent variables. If the VIF exceeds 10, the regression model has a severe multicollinearity problem, and the variable should not be included in the regression (Vittinghoff et al., 2012).

3. Results

3.1. Residential CO_2 emissions pattern in the urban center regions

The intensity and summary of the 31 cities' CO_2 emissions were not significantly different. In Fig. 3, Beijing (Type I) was the first and second greatest city in emission summary and intensity, respectively. Kunming (Type II) had relatively small total and medium mean emissions. The emission intensity of the Type III cities was higher than the Type IV cities. The total emissions of the Type III cities were slightly lower than the Type IV cities. Shanghai emitted the second largest CO_2 among 31 cities. With the greatest emission intensity, Shanghai was about six times higher than that of Yantai, which was the lowest. It is worth noting that the Xiamen and Wuhan had relatively high intensity and total emissions. The standard deviations of the great emission intensity cities were large. Except for Yantai, the other 30 cities had pixel values of CO_2 emissions larger than 1000 t/km^2. Most of the pixel values of the 31 cities were scattered, except for Xiamen and Yantai of the Type III city and Dalian, Guiyang, Nanning, Tangshan, and Xi'an of the Type IV city (Figure A3).

The Moran's I of the four cities types ranged from 0.473 to 0.911, showing no significant difference (Fig. 4). Chongqing (0.911) and Yantai (0.883) from the Type II city were the top two highest Moran's I values cities. Tangshan (0.473), Harbin (0.564), and Shijiazhuang (0.597) belonged to the Type IV city were the three lowest Moran's I values cities. Besides, there were significant statistical differences in the proportion of cold-hot spots in the four cities types (Figure A4). The hot and cold spot areas of most Type III cities were smaller than the other three types of cities. It represented that the aggregation pattern of the Type III city was relatively weak. Kunming (Type II), Shijiazhuang (Type IV), and Tangshan (Type IV), which didn't have significant total emissions, had a high proportion of hot spots with 31.4%, 42.2%, and 35.9%, respectively. The cold spot proportions in some cities were close to 0 (e.g., Wuxi, Changchun, Ningbo, Xiamen, Tianjin, and Wuxi).

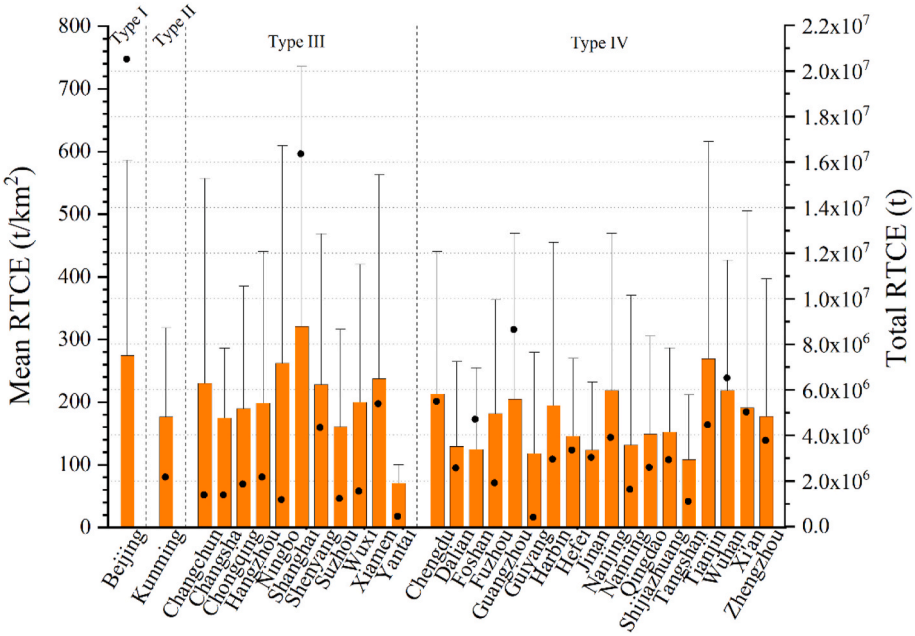

Fig. 3. The mean (left axis with bar and standard error) and total (right axis with point) residential CO_2 emissions in 31 cities.

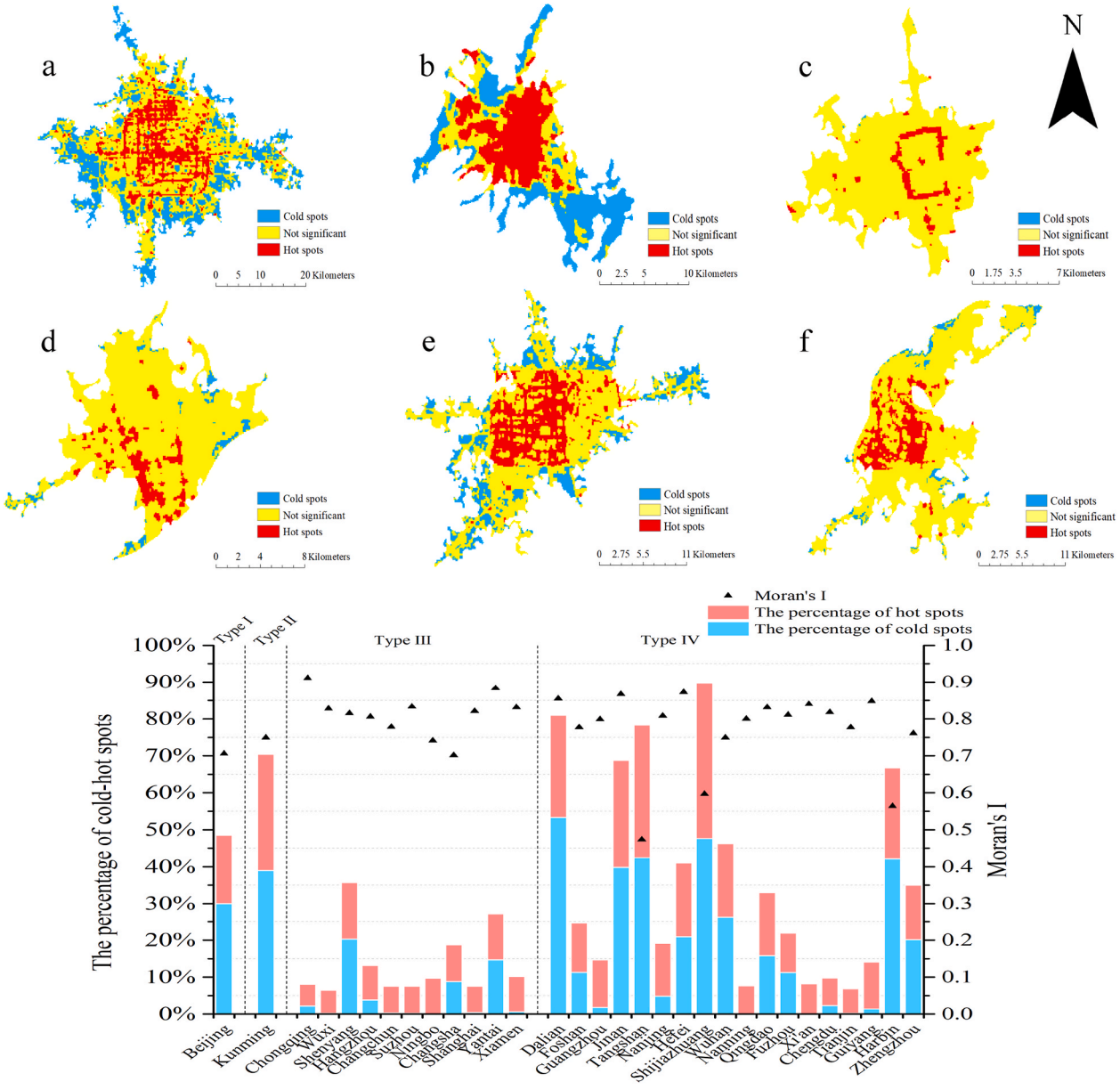

Fig. 4. The cold and hot spots map of the residential CO_2 emissions in a. Beijing (Type I), b. Kunming (Type II), c. Suzhou (Type III), d. Hangzhou (Type III), e. Hefei (Type IV), f. Nanjing (Type IV), the Moran's I and area proportion of cold and hot spots in 31 cities.

3.2. Descriptive analysis of urban forms indicators

Beijing and Kunming were the only cities in Type I and II, respectively. Beijing's green space area ratio (146438.27 m^2/km^2) and road length density (16061.99 m/km^2) were high. While the functional mixed entropy (FME), building area, and building floor were low at 0.088, 20572.551$m^2/km,^2$ and 381.842 $floor/km,^2$ respectively. The FME (1.406) and bus station density (5.412 per km^2) of Kunming were high. In contrast, the values of other indicators were low. There were significant differences between Type III (11 cities) and Type IV (17 cities), except for the green space density (Table A2). The Type III city (e.g., Suzhou, Hangzhou, and Shanghai) had higher values of bus station (6.918–2.613 per km^2), road intersection (266.439–88.638 per km^2), road length (18258.275–14662.198 m/km^2), building area (245688.418–162160.231 m^2/km^2), building shape index (1.142–0.918), building floor (6431.148–469.645 $floor/km^2$) and FME (1.051–0.114) than the Type IV cities (e.g., Shijiazhuang, Hefei, Nanning). However, the green space density and FME of the Type III city were much lower than of Beijing and Kunming. The eight indicators of the urban form of Type IV city were lower than the overall average level (Fig. 5).

From the perspective of different functional area proportions (Fig. 6), the residential zone occupied the highest area proportion in the 31 cities. The average residential zone proportions of the four types of cities were 46.93%, 32.90%, 46.86%, and 41.38%, respectively. The residential zone proportions of some cities were relatively minor, such as Yantai (16.19%) and Nanning (17.81%). Chongqing (68.86%) and Guiyang (61.42%) had relatively large residential zones. Except for Beijing, the park & greenspace zone was the smallest functional zone for the other type of cities. The transportation and park & greenspace zones accounted for 19.90% and 14.33% of the area in Beijing (Type I) and 28.68% and 12.07% in Kunming (Type II), respectively. The Type III, which included the representative cities of Hangzhou and Suzhou, had the mean proportion of industrial zones (17.48%), transportation zones (14.05%), and commercial zones (10.35%). The mean area proportion of industrial zones (19.32%) was slightly higher than transportation

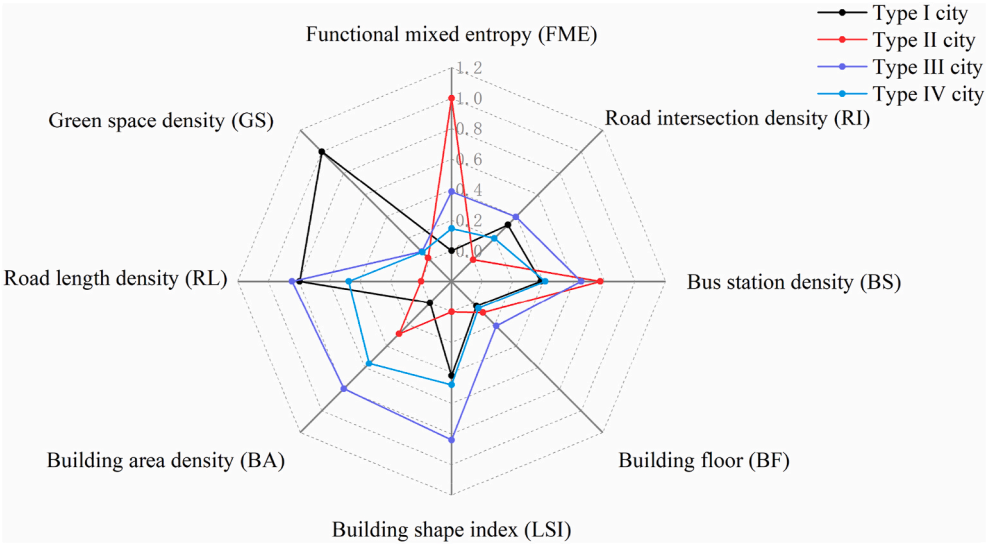

Fig. 5. The classifications of the 31 cities via urban form indicators. The Type I city only includes Beijing. The Type II city only includes Kunming. The Type III city includes Chongqing, Wuxi, Shenyang, Hangzhou, Changchun, Suzhou, Ningbo, Changsha, Shanghai, Yantai, and Xiamen. The Type IV city includes Dalian, Foshan, Guangzhou, Jinan, Tangshan, Nanjing, Hefei, Shijiazhuang, Wuhan, Nanning, Qingdao, Fuzhou, Xi'an, Chengdu, Tianjin, Guiyang, Harbin, and Zhengzhou.

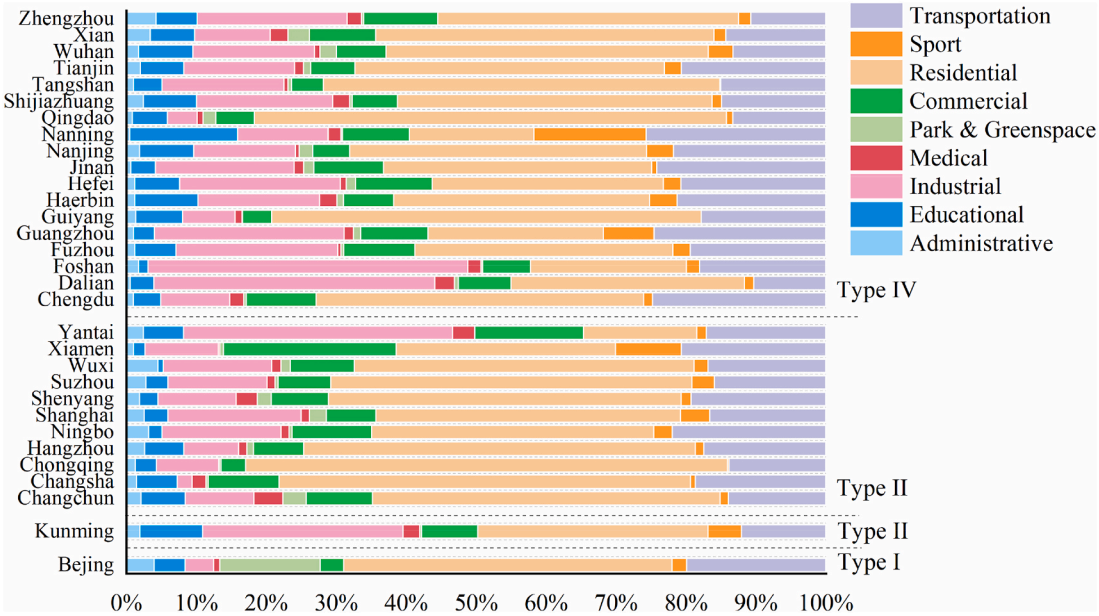

Fig. 6. Area proportions of the different functional zones.

zones (18.38%) among the Type IV city which included the representative cities such as Nanjing, Hefei, and Shijiazhuang.

3.3. Impacts of urban forms on RTCE

GWR model has different independent variables in different cities (Table A4). The results showed that the eight indicators accounted for 45.9% of RTCE. The mean R^2 of the four types of cities were 0.356, 0.543, 0.432, and 0.476, respectively. The difference was not significant. The rank of average regression coefficients (ARC) was FME > LSI > BS > RI > BF > RL > GS > BA.

The ARC of FME was positive in most functional zones of most cities but negative in some zones (e.g., the business zone of Xiamen, the industrial zone of Chongqing, the medical zone of Shijiazhuang, the green space zone of Changsha and Chongqing, and the sport of Changsha) (Figure A5). It means that FME had the greatest positive influence in most cities. However, there is an opposite trend in some different functional areas. The FME had the greatest influence on the administrative zone and the least on the medical zone for the Type I city. As to the other three types, the great influence appeared in the sport, followed by the administrative zone. The industrial zone has the least influence on the FME. It showed that the urban form of Type I may be quite different from the other three types.

The Type I city (only Beijing) had low FME (0.088) and higher ARC (Range: 93.97 to 9860.95, Mean:151.22) in nine functional zones than those of the other three types of cities. The Type II city (only Kunming) had the high FME (1.406) and lower ARCs (Range: 0.84 to 2.97, Mean: 1.66) in the nine functional zones than cities of the other three types. The mean FME of the Type III city (0.60) was higher than that of the Type IV city (0.29), but the ARCs (Range: 15.49 to 29.65) in the nine functional zones were lower than that in the Type IV city (Range: 28.39 to38.62). Therefore, we preliminary inferred that the region with low

FME greatly influenced RTCE. However, with the increase of FME, its influence decreased continuously, which indicated that the city with the highest FME had the smallest ARC value. Based on the ARCs and FMEs of 31 cities, the exponential function with 0.792 R^2 was the best fitting equation. When the FME was less than 0.28, the regression coefficient decreased sharply and then decreased gradually with the FME increased. It meant that the increase of FME significantly impacted RTCE when it was less than 0.28, and then the influence decreased (Fig. 7).

In general, although the ARC of building shape index (LSI) was positive in most cases, the more complex the building shape with considerable LSI value, the greater the RTCE (Figure A6). That is, when the 2D shape of a building is relatively simple, the influence on RTCE is greater. However, the influence becomes complicated with the irregularity of the building. Except for that, the ARCs of some functional zones (except green land and industrial land) were negative, such as the commercial zone in the Type III and IV cities, indicating that the larger the LSI value, the less RTCE.

The ARC of bus station density (BS) was less than 1.0 in different functional zones of most cities (Figure A7). The Type II cities had the largest BS value (5.41 per km^2) and large ARC. However, the other types of cities didn't show a similar relation. BS has a greater impact on the increase of RTCE in the park & green space, the commercial and educational zones than the other functional zones.

Referring to RI variable, the absolute value of the ARC of each functional zone ranged from 0.004 to 0.046 (Figure A8). The ARCs of medical and educational zones in Beijing and Kunming were both negative. Shanghai, a city with the highest RI (266.44/km^2), had negative ARC in all the nine functional zones. However, regression coefficients' effect directions in other cities were various in different functional zones. The ARCs of FL, RL, GS, and BA were small, with absolute values ranging from 0.001 to 0.035, 0.001–0.002, 0.00–0.001, and 0.00–0.005, respectively (Figure A9-A12). The FL's ARCs of Suzhou (Type III), Dalian (Type IV), Guiyang (Type IV), Qingdao (Type IV), and Tianjin (Type IV), the RL's ARCs of Guiyang (Type IV) and Suzhou (Type III) were all negative in the nine functional zones. Only two cities (Ningbo and Xiamen) had the GS variables in the regression with negative coefficients.

4. Discussion

4.1. 1The factors affect the residential CO_2 emissions

The research findings at the national, provincial, and city scales indicate that different urban spatial factors, which can be divided into direct and indirect factors, have a significant impact on RTCE. Our result is consistent with the prior study that about 50% of urban CO_2 emissions can be attributed to urban form, land mix, building types, and transport networks (Christen et al., 2011). Except for that, the economic, population, and urban area sprawl were the significant factors accelerating the urban CO_2 emission. From the regional scale, urbanization positively affects CO_2 emissions through a series of approaches (Cheng and Hu, 2022; Shi et al., 2020a,b; Wang et al., 2018). Shi et al. (2020a,b) found that the urban area, economic structure, and population could affect the CO_2 emission based on the 264 Chinese cities data from 2000 to 2015. Fan et al. (2017) used the Divisa decomposition method to find that urban-rural population structure facilitated the residential energy consumption structure improvement. The GDP, tertiary industry ratio, and energy intensity could also influence the RTCE (Su and Lee, 2021). Because the economic level determines the residential income and living conditions. From the individual scale, the social factors such as the educational level, building characteristics and the degree of aging, travel instrument preference, travel distance, family condition, and community type affected the RTCE. Moreover, upon referencing previous studies, the precipitation impacts the RTCE due to the choice of the travel instrument (Fan et al., 2018; Kashifi et al., 2022; Shi et al., 2019). Besides, the green space in urban regions has the positive effects on CO_2 emissions might be due to the residents' preference and aggregation. The temperature affects the energy used for heating and cooling.

Among the urban form indicators, RL, BS, and BA represent urban scale effect and development intensity. We found that an increase of 1 unit intensity per square kilometer of the three indicators had minor impacts on RTCE. It may be due to the magnitude difference caused by the non-normalization of the independent variables. The scale effect indicators lead to two sides of the influence on RTCE. On the one hand, the increase of construction land promoted the expansion of the urban center to the suburbs and increased the distance of traffic travel and the absorption of the solar heat resulting in the increase of RTCE. On the other hand, optimizing the construction of the urban center may

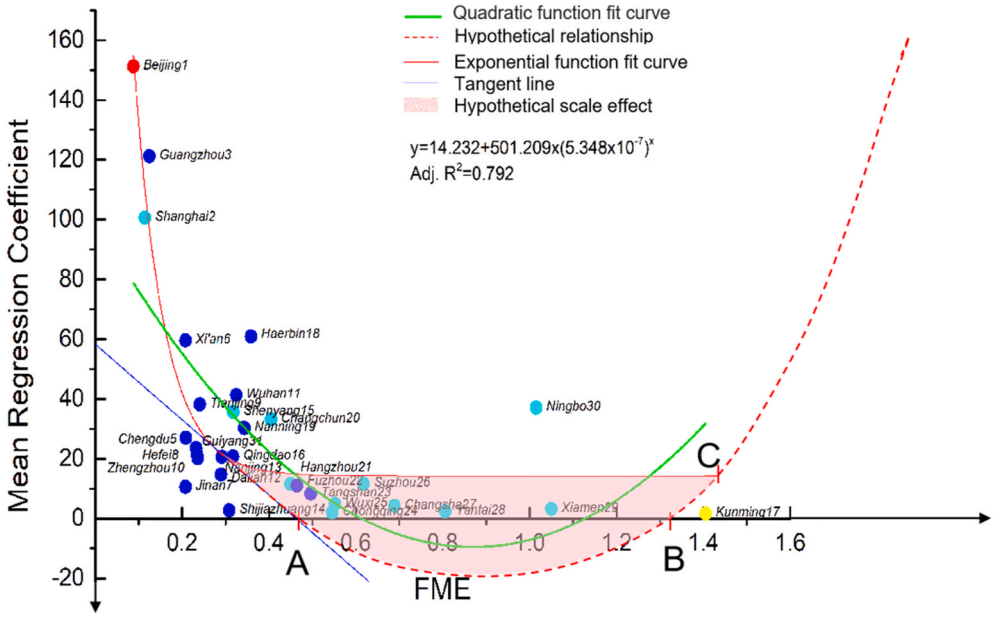

Fig. 7. The relation between the functional mixed entropy and the GWR mean regression coefficients in 31 cities. The red, yellow, light blue and blue dot represents the Type I, II, III and IV city, respectively. The numbers follow the city names represent the size order of the urban area. Point A, B and C are hypothetical.

alleviate traffic congestion, increase accessibility, and reduce urban heat island effect leading to the decrease of RTCE (Choi and Zhang, 2017a).

As to urban external morphology indicators (LSI and BF), we found that in most cases, the more complex the 2D shape of the building, the greater the RTCE. The result was consistent with previous studies, which showed that no matter 3D building shapes, land use patch shapes, complexity, irregular and dispersed shapes (represented by Edge Density (ED), Landscape Shape Index (LSI), Fractal Dimension Index (FRAC) or Building Shape Coefficient (BSC)) would lead to more CO_2 emissions. For the 3D morphology of the individual building, the larger heat dissipation area and raised temperature results in high energy consumption (Xu et al., 2021). The complex shape of the building means more adjacencies with soil cover, which have a substantial effect on the increase in land surface temperature (Azhdari et al., 2018; Hu et al., 2022). For city-level CO_2 emissions, studies on urban land patch shape complexity represented by ED indicated that scattered and irregular land use was associated with increased CO_2 emission levels (Wang et al., 2017). Xia et al. (2017) found that the center region of Beijing with the most CO_2 emissions was more complicated than the suburban and exurban regions. In addition, we found that one-third of commercial zones in the 31cities showed that the more complex the building shape was, the less RTCE emitted. It might be due to the potential public transportation requirement resulting from large commercial zones with complex shape (Ou et al., 2019). Similar to the building shape influence, the ARC of building height is positive in more than two third of the cities, indicating that in most cases, building height had a positive impact on RTCE. This is consistent with early results, in which taller buildings got more daylight and solar energy and increased the risk of overheating. Moreover, the operation of ventilation equipment and elevator increased the energy consumption, thus offsetting the energy saving caused by the increase in illumination time (Borck, 2016). Building height affected the thermal environment and solar access, affecting CO_2 emissions in densely packed regions (Kaspersen et al., 2016). However, the life cycle assessment method found that for commercial buildings less than 12 floors, the impact of building height was small, mainly relying on technical system solutions to reducing energy consumptions. CO_2 emissions increased slightly from buildings wiht 12 to 21 floors. A study of office building emissions found that average carbon emissions would increase more than doubled when the building height rising from 5 floors and below to 21 floors and above (Godoy--Shimizu et al., 2018).

The FME, BS, and RI, which represent the internal characteristics of urban form, directly influenced the residential travel accessibility and efficiency. Although most studies showed that public transportation system reduced CO_2 emissions from travel. Its impact is neither absolute nor direct. The service efficiency of public transport (e.g., accessibility of the BS and route design of the RI) is the key to different results. We found that in densely populated areas, there is greater demand for public transit stations to access parks, commercial and educational zones. Furthermore, the increase in travel emissions when adding one bus station per square kilometer, the increase of travel emissions was also greater. It corresponded with the study, which showed that the number of buses positively impacted CO_2 emissions from transport (Sun et al., 2019). Through Eddy Covariance (EC) measurements of CO_2 flux (FC), it is found that the main sources of CO_2 emissions in the urban area of the city of Heraklion come from the main roads and intersections with heavy traffics (Stagakis et al., 2019). The number of intersections affects the accessibility of surrounding service facilities, the speed of vehicles, and the degree of congestion, thus affecting CO_2 emissions (Massar et al., 2021). Through model simulation and field measurement, scholars found that transforming two-way parking controlled intersections into roundabouts in highest traffic volume scenarios can reduce vehicle emissions (Gastaldi et al., 2017; Yang et al., 2017). However, some studies suggest that different types of intersections have different impacts on CO_2 emissions under different restrictions (e.g., Arterial level) (Fernandes et al., 2019). Shanghai, the city with the highest intersection density (266.44 per km^2), has negative average regression coefficients in all nine functional zones, but the effect directions of regression coefficients in other cities are different in various functional zones. This irregularity may be caused by not distinguishing different types of intersections. Further studies can be conducted to explore the impact of different intersections on the urban scale.

4.2. Impacts of the FME on RTCE

A large amount of the previous studies were conducted at individual and household scales. Scholars revealed that high-density and mixed land use could improve accessibility so that high-density and mixed land use mitigated transport CO_2 emissions, especially per capita emissions, while the densification and mixed-use development might also lead to slow vehicle speeds and more vehicle emissions at the individual and household scale (Son et al., 2018). Land use affects travel costs through distance and time consumption. When the costs fall, people prefer walking, biking or taking public transport. Moreover, to a certain extent, land use changes transportation emissions by influencing vehicle miles traveled (VMT). Even after controlling traveler preferences, the effect of urban form on the transportation emission was still significant, which was larger than 50% on VMT. However, the relationship direction between land use and travel changed to a different direction at a large geographical scale. Some results showed that families might frequently take short-distance vehicle trips even if they lived in areas with high mixed density or good job-housing balance (Nasri and Zhang, 2015). CO_2 emissions in mixed-use buildings are higher than in general residential buildings (Choi and Zhang, 2017b). Because the vehicle travel emissions were influenced by local urban form factors and the large geographical environment. The accessibility in the city context had a greater impact than on individual and local scale projects. The influence of the urban form of adjacent areas depends on the urban spatial context and transportation infrastructure (Choi and Zhang, 2017a; de Koning et al., 2020; Lee and Lee, 2020; Soliz, 2021). The metropolitan city can disperse the various functional areas to the newly developed region (Fang and Yu, 2017). This could explain our findings that the mixing entropy of central metropolitan areas such as Beijing, Shanghai, and Guangzhou was low but had a significant influence on the RTCE at the regional scale. This study found that the influence of the FME on the RTCE was positive. With the increased FME, the influence power gradually reduced in cities such as Kunming, Xiamen, and Ningbo which have the small central region area and high FME values. The reason might be that the growth of emissions was offset by the efficiency from the economic scale (e.g., population and resources) effect. The mixed-use of residential, commercial, and office space had co-benefits, including boosting the local economy, providing public services and community support, and reducing landscape fragmentation (Abubakar and Dano, 2019). This compact form favored non-motorized transport (e.g., walking and cycling) and supported the development of public transportation (Kammen and Sunter, 2016). The degree of mix should have a reasonable range. Based on multi-scale studies, scholars believed there might be a U-shaped curve between urban population density and residents' direct traffic emissions (Zhang et al., 2015). We assumed that the law found in this study conformed to the downward trend of the left half of the curve. However, the upward trend of the right half has not yet been shown because of a lack of experimental data (Fig. 7). Suppose we used the quadratic function to test the probability of the U-shaped based on the existing 31 cities data (Lind and Mehlum, 2010). The quadratic term was significant (P value $0.002 < 0.01$) despite the 0.463 R2. The estimated extremum point of FME (0.872) was in a reasonable interval [0.088, 1.406], which was the range of 31 FMEs. The slope at FME equal to 0.088 was −225.750, and the slope at FME equal to 1.406 was 154.520. The slope of the tangent decreased when FME was less than 0.872 and vice versa. The results demonstrated that the curve was U-shaped in the range of existing data. Theoretically, when the efficiency of the urban scale effect represented by population density and

building density was stripped, and the FME was larger than point A, the ARC of FME would be negative. The scale effect efficiency increased first and then decreased, leading to the optimal maximum value of the FME at point B (without the scale effect) and C (with the scale effect). However, we weren't sure where the point C would be in this study, Because there were a few cities with FME larger than 0.8. We suggested that cities with regional FME below 0.28 increase the FME appropriately to reduce the influence, cities with FME near 0.28 maintain the FME, and cities with FME above 0.80 (Yantai, Xiamen, Ningbo, and Kunming) should consider reducing or maintaining the FME. Because the average FME of a small number of cities was greater than 1.0. Although Xiamen and Kunming were in line with the trend of the fitting curve, Ningbo showed high FME and strong influence.

4.3. Significance, limitation and recommendation

Through the spatial analysis, this study demonstrates the impacts of Chinese urban center spatial forms on residential and transport CO_2 emissions at the grid scale. The strengths are as follows: (1) This study is one of few studies to connect the large (city, provincial, and national) and small (community, block, and individual) scales. (2) Spatial analysis, which is different from ordinary linear and time series analysis, considers the spatial location information of urban form. (3) The rule we discovered about the influence of FME on RTCE can guide the development of some regional land use policy tools.

This study also has a number of limitations. First, the study, which was on the urban scale, didn't consider personal behavior factors. Therefore, the study was based on the hypothesis that the environment drives personal behaviors. (2) The independent variables of GWR analysis were not dimensionless, which may lead to lower regression coefficients of some impact factors. But the regression results were easy to interpret. (3) The small grid obtained by downscaling interpolation may influence the research results.

We suggested that more empirical data should be collected in the future to further study the influence of FME on RTCE in different urban areas in order to demonstrate whether the hypothetical inverse hump-shaped or U-shaped curve exists. In addition, the influences of configuration and composition of different functional areas should be further discussed. Furthermore, the selection of indicators for urban interior features can be further discussed, such as the selection of the new and more representative indicators and the detailed classification of FME, intersection points, and bus station data. Lastly, the analysis result of GWR is based on the cross-sectional data. When the data is available,the cause-and-effect relationship could be tested in further research by using methods such as geographical and temporal weighted regression (GTWR). Meanwhile, the other method to test the cause-and effect relationship is field observation and investigation by eddy covariance.

5. Conclusion

Most of the existing research focused on scales larger than the city or smaller than the local region. In this study, we investigated the association between the urban form and RTCE based on experimental data of the 31 cities and revealed that internal urban characteristics were important.

The research results found that most city forms were similar among the 31 city centers based on the eight indicators. The Type III city centers had higher indicator values than Type IV city, which indicated more mature infrastructure in the Type III city. Type III city had higher emission intensity and slightly lower total emissions than Type IV city. This is, probably due to the city scale effect. Moreover, the CO2 emission aggregation pattern of the Type III city was relatively weak.

In addition to the urban form characteristics, we found that the eight urban form indicators explained about 45.9% of RTCE. The rank of ARC was FME > LSI > BS > RI > BF > RL > GS > BA. The internal characteristics indicators (FME, BS, and RI) had significant influences on RTCE. The influence of FME on RTCE would decreased with the increase of the FME value based on the fitting exponential function.

Another finding was that the ARC of FME was positive in most functional zones of most cities. The influence of the FME on RTCE would decrease with the increase of the FME value based on the fitting exponential function. Therefore, we suggested that cities with FME below 0.28 increase it appropriately to reduce the influence, and cities with FME near 0.28 maintain it. We assumed that the pattern found in this study conformed to the downward trend of the left half of the U-shaped curve. Cities with FME above 0.80 (Yantai, Xiamen, Ningbo, and Kunming) should consider to reduce or maintain it.

Besides FME, in most cities, the RTCE increased with the complexity of the 2D shape of the building growing. The simple shape had a great influence on RTCE. However, the influence became more complicated when the form turned irregular.

CRediT authorship contribution statement

Shudi Zuo: Conceptualization, Methodology, Formal analysis, Writing – original draft, Writing – review & editing. **Shaoqing Dai:** Data curation, Writing – review & editing. **Jiaheng Ju:** Visualization, Data curation, Formal analysis, Writing – review & editing. **Fanxin Meng:** Resources. **Yin Ren:** Supervision. **Yunfeng Tian:** Data curation. **Kaide Wang:** Resources.

Declaration of competing interest

The authors declare that they have no known competing financial interests or personal relationships that could have appeared to influence the work reported in this paper.

Data availability

Data will be made available on request.

Acknowledgments

This work was supported by National Natural Science Foundation of China (42001210, 31972951, 31670645, 42171100, 41801182, and 41807502), National Social Science Fund of China (17ZDA058), Fujian Provincial Department of S&T Project (2022T3047, 2021I0041, 2021T3058, 2019J01136). We are grateful to the anonymous reviewers for their constructive suggestions.

Appendix A. Supplementary data

Supplementary data to this article can be found online at https://doi.org/10.1016/j.jclepro.2022.134947.

References

Abubakar, I.R., Dano, U.L., 2019. Sustainable urban planning strategies for mitigating climate change in Saudi Arabia. Environ. Dev. Sustain. 22 (6), 5129–5152. https://doi.org/10.1007/s10668-019-00417-1.

Azhdari, A., Soltani, A., Alidadi, M., 2018. Urban morphology and landscape structure effect on land surface temperature: evidence from Shiraz, a semi-arid city. Sustain. Cities Soc. 41, 853–864. https://doi.org/10.1016/j.scs.2018.06.034.

Borck, R., 2016. Will skyscrapers save the planet? Building height limits and urban greenhouse gas emissions. Reg. Sci. Urban Econ. 58, 13–25. https://doi.org/10.1016/j.regsciurbeco.2016.01.004.

Cheng, Z., Hu, X., 2022. The effects of urbanization and urban sprawl on CO_2 emissions in China. Environ. Dev. Sustain. https://doi.org/10.1007/s10668-022-02123-x.

Choi, K., Zhang, M., 2017a. The impact of metropolitan, county, and local land use on driving emissions in US metropolitan areas: mediator effects of vehicle travel characteristics. J. Transport Geogr. 64, 195–202. https://doi.org/10.1016/j.jtrangeo.2017.09.004.

Choi, K., Zhang, M., 2017b. The net effects of the built environment on household vehicle emissions: a case study of Austin, TX. Transp. Res. D. Transp. Environ. Times 50, 254–268. https://doi.org/10.1016/j.trd.2016.10.036.

Christen, A., Coops, N.C., Crawford, B.R., Kellett, R., Liss, K.N., Olchovski, I., Tooke, T.R., van der Laan, M., Voogt, J.A., 2011. Validation of modeled carbon-dioxide emissions from an urban neighborhood with direct eddy-covariance measurements. Atmos. Environ. 45 (33), 6057–6069. https://doi.org/10.1016/j.atmosenv.2011.07.040.

de Koning, R., Tan, W.G.Z., van Nes, A., 2020. Assessing spatial configurations and transport energy usage for planning sustainable communities. Sustainability 12 (19). https://doi.org/10.3390/su12198146.

Ewing, R., Rong, F., 2008. The impact of urban form on U.S. residential energy use. Hous. Policy Deb 19 (1), 1–30. https://doi.org/10.1080/10511482, 2008.9521624.

Fan, C., Myint, S., 2014. A comparison of spatial autocorrelation indices and landscape metrics in measuring urban landscape fragmentation. Landsc. Urban. Plan 121, 117–128. https://doi.org/10.1016/j.landurbplan.2013.10.002.

Fan, C., Tian, L., Zhou, L., Hou, D., Song, Y., Qiao, X., Li, J., 2018. Examining the impacts of urban form on air pollutant emissions: evidence from China. J. Environ. Manag. 212, 405–414. https://doi.org/10.1016/j.jenvman.2018.02.001.

Fan, J.-L., Zhang, Y.-J., Wang, B., 2017. The impact of urbanization on residential energy consumption in China: an aggregated and disaggregated analysis. Renew. Sust. Energy Rev. 75, 220–233. https://doi.org/10.1016/j.rser.2016.10.066.

Fang, C.L., Yu, D.L., 2017. Urban agglomeration: an evolving concept of an emerging phenomenon. Landsc. Urban Plann. 162, 126–136. https://doi.org/10.1016/j.landurbplan.2017.02.014.

Fernandes, P., Fontes, T., Neves, M., Pereira, S.R., Bandeira, J.M., Rouphail, N.M., Coelho, M.C., 2019. Assessment of corridors with different types of intersections. Transport. Res. Rec. 2503 (1), 39–50. https://doi.org/10.3141/2503-05.

Feyisa, G.L., Dons, K., Meilby, H., 2014. Efficiency of parks in mitigating urban heat island effect: an example from Addis Ababa. Landsc. Urban Plann. 123, 87–95. https://doi.org/10.1016/j.landurbplan.2013.12.008.

Gastaldi, M., Meneguzzer, C., Giancristofaro, R.A., Gecchele, G., Della Lucia, L., Prati, M. V., 2017. On-road measurement of CO_2 vehicle emissions under alternative forms of intersection control. 20th Euro Work. Group Transport. Meet. 476–483.

Geng, Y., Chen, W., Liu, Z., Chiu, A.S.F., Han, W., Liu, Z., Zhong, S., Qian, Y., You, W., Cui, X., 2017. A bibliometric review: energy consumption and greenhouse gas emissions in the residential sector. J. Clean. Prod. 159, 301–316. https://doi.org/10.1016/j.jclepro.2017.05.091.

Godoy-Shimizu, D., Steadman, P., Hamilton, I., Donn, M., Evans, S., Moreno, G., Shayesteh, H., 2018. Energy use and height in office buildings. Build. Res. Inf. 46 (8), 845–863. https://doi.org/10.1080/09613218.2018.1479927.

Gong, P., Chen, B., Li, X., Liu, H., Wang, J., Bai, Y., Chen, J., Chen, X., Fang, L., Feng, S., Feng, Y., Gong, Y., Gu, H., Huang, H., Huang, X., Jiao, H., Kang, Y., Lei, G., Li, A., Li, X., Li, X., Li, Y., Li, Z., Li, Z., Liu, C., Liu, C., Liu, M., Liu, S., Mao, W., Miao, C., Ni, H., Pan, Q., Qi, S., Ren, Z., Shan, Z., Shen, S., Shi, M., Song, Y., Su, M., Ping Suen, H., Sun, B., Sun, F., Sun, J., Sun, L., Sun, W., Tian, T., Tong, X., Tseng, Y., Tu, Y., Wang, H., Wang, L., Wang, X., Wang, Z., Wu, T., Xie, Y., Yang, J., Yang, J., Yuan, M., Yue, W., Zeng, H., Zhang, K., Zhang, N., Zhang, T., Zhang, Y., Zhao, F., Zheng, Y., Zhou, Q., Clinton, N., Zhu, Z., Xu, B., 2020. Mapping essential urban land use categories in China (EULUC-China): preliminary results for 2018. Sci. Bull. 65 (3), 182–187. https://doi.org/10.1016/j.scib.2019.12.007.

Hu, D., Meng, Q., Schlink, U., Hertel, D., Liu, W., Zhao, M., Guo, F., 2022. How do urban morphological blocks shape spatial patterns of land surface temperature over different seasons? A multifactorial driving analysis of Beijing, China. Int. J. Appl. Earth Obs. Geoinf. 106 https://doi.org/10.1016/j.jag.2021.102648.

Jiang, W., He, G., Long, T., Guo, H., Yin, R., Leng, W., Liu, H., Wang, G., 2018. Potentiality of using Luojia 1-01 nighttime light imagery to investigate artificial light pollution. Sensors 18 (9), 2900. https://doi.org/10.3390/s18092900.

Kammen, D.M., Sunter, D.A., 2016. City-integrated renewable energy for urban sustainability. Science 352 (6288), 922–928. https://doi.org/10.1126/science.aad9302.

Kashifi, M.T., Mansoor, U., Rahman, S.M., 2022. Transit leverage assessment and climate change mitigation pathway for urbanised areas. Int. J. Glob. Warming 26 (1), 18–37. https://doi.org/10.1504/ijgw.2022.120066.

Kaspersen, B., Lohne, J., Bohne, R.A., 2016. Exploring the CO_2-impact for building height; A study on technical building installations. Energy Proc. 96, 5–16. https://doi.org/10.1016/j.egypro.2016.09.089.

Knappe, J., Somlai, C., Gill, L.W., 2022. Assessing the spatial and temporal variability of greenhouse gas emissions from different configurations of on-site wastewater treatment system using discrete and continuous gas flux measurement. Biogeosciences 19 (4), 1067–1085. https://doi.org/10.5194/bg-19-1067-2022.

Larsson, J., Elofsson, A., Sterner, T., Akerman, J., 2019. International and national climate policies for aviation: a review. Clim. Pol. 19 (6), 787–799.

Lee, S., Lee, B., 2014. The influence of urban form on GHG emissions in the U.S. household sector. Energy Pol. 68, 534–549. https://doi.org/10.1016/j.enpol.2014.01.024.

Lee, S., Lee, B., 2020. Comparing the impacts of local land use and urban spatial structure on household VMT and GHG emissions. J. Transport Geogr. 84 https://doi.org/10.1016/j.jtrangeo.2020.102694.

Li, X., Gong, P., Zhou, Y., Wang, J., Bai, Y., Chen, B., Hu, T., Xiao, Y., Xu, B., Yang, J., Liu, X., Cai, W., Huang, H., Wu, T., Wang, X., Lin, P., Li, X., Chen, J., He, C., Li, X., Yu, L., Clinton, N., Zhu, Z., 2020. Mapping global urban boundaries from the global artificial impervious area (GAIA) data. Environ. Res. Lett. 15 (9) https://doi.org/10.1088/1748-9326/ab9be3, 094044.

Lind, J.T., Mehlum, H., 2010. With or without U? The appropriate test for a U-shaped relationship. Oxf. Bull. Econ. Stat. 72 (1) https://doi.org/10.1111/j.1468-0084.2009.00569.x, 0305–9049.

Liu, J.H., Li, M.X., Ding, Y.T., 2021. Econometric analysis of the impact of the urban population size on carbon dioxide (CO_2) emissions in China. Environ. Dev. Sustain. 23 (12), 18186–18203. https://doi.org/10.1007/s10668-021-01433-w.

Liu, L.C., Wu, G., Wang, J.N., Wei, Y.M., 2011. China's carbon emissions from urban and rural households during 1992-2007. J. Clean. Prod. 19 (15), 1754–1762. https://doi.org/10.1016/j.jclepro.2011.06.011.

Liu, Z., Guan, D., Wei, W., Davis, S.J., Ciais, P., Bai, J., Peng, S., Zhang, Q., Hubacek, K., Marland, G., Andres, R.J., Crawford-Brown, D., Lin, J., Zhao, H., Hong, C., Boden, T. A., Feng, K., Peters, G.P., Xi, F., Liu, J., Li, Y., Zhao, Y., Zeng, N., He, K., 2015. Reduced carbon emission estimates from fossil fuel combustion and cement production in China. Nature 524 (7565), 335–338. https://doi.org/10.1038/nature14677.

Massar, M., Reza, I., Rahman, S.M., Abdullah, S.M.H., Jamal, A., Al-Ismail, F.S., 2021. Impacts of autonomous vehicles on greenhouse gas emissions-positive or negative? Int. J. Environ. Res. Publ. Health 18 (11). https://doi.org/10.3390/ijerph18115567.

Meijer, J.R., Huijbregts, M.A.J., Schotten, K.C.G.J., Schipper, A.M., 2018. Global patterns of current and future road infrastructure. Environ. Res. Lett. 13 (6) https://doi.org/10.1088/1748-9326/aabd42.

Meng, S.a., Zacharias, J., 2021. Street morphology and travel by dockless shared bicycles in Beijing, China. Int. J. Sustain. Transp 15 (10), 788–798.

Molla, A., Zuo, S.D., Zhang, W.W., Qiu, Y., Ren, Y., Han, J.G., 2022. Optimal spatial sampling design for monitoring potentially toxic elements pollution on urban green space soil: a spatial simulated annealing and k-means integrated approach. Sci. Total Environ. 802 https://doi.org/10.1016/j.scitotenv.2021.149728.

Nasri, A., Zhang, L., 2015. Assessing the impact of metropolitan-level, county-level, and local-level built environment on travel behavior: evidence from 19 U.S. urban areas. J. Urban Plann. Dev. Div., Am. Soc. Civ. Eng 141 (3). https://doi.org/10.1061/(asce)up.1943-5444.0000226.

Oliveira, V., 2019. An historico-geographical theory of urban form. J. Urbanism 12 (4), 412–432. https://doi.org/10.1080/17549175.2019.1626266.

Ou, J., Liu, X., Li, X., Chen, Y., 2013. Quantifying the relationship between urban forms and carbon emissions using panel data analysis. Landsc. Ecol. 28 (10), 1889–1907. https://doi.org/10.1007/s10980-013-9943-4.

Ou, J.P., Liu, X.P., Wang, S.J., Xie, R., Li, X., 2019. Investigating the differentiated impacts of socioeconomic factors and urban forms on CO_2 emissions: empirical evidence from Chinese cities of different development levels. J. Clean. Prod. 226, 601–614. https://doi.org/10.1016/j.jclepro.2019.04.123.

Pivo, G., Frank, L.D., 1994. Impacts of mixed use and density on utilization of three modes of travel: single-Occupant Vehicle, Transit, and Walking. Transport. Res. Rec. 1466, 44–52.

Santos, T., Deus, R., Rocha, J., Tenedório, J.A., 2021. Assessing sustainable urban development trends in a dynamic tourist coastal area using 3D spatial indicators. Energies 14 (16), 5044. https://doi.org/10.3390/en14165044.

Sharifi, A., 2019. Urban form resilience: a meso-scale analysis. Cities 93, 238–252. https://doi.org/10.1016/j.cities.2019.05.010.

Sharifi, A., Wu, Y., Khamchiangta, D., Yoshida, T., Yamagata, Y., 2018. Urban carbon mapping: towards a standardized framework. Energy Proc. 152, 799–808. https://doi.org/10.1016/j.egypro.2018.09.193.

Shi, K., Xu, T., Li, Y., Chen, Z., Gong, W., Wu, J., Yu, B., 2020a. Effects of urban forms on CO_2 emissions in China from a multi-perspective analysis. J. Environ. Manag. 262 https://doi.org/10.1016/j.jenvman.2020.110300.

Shi, K., Xu, T., Li, Y., Chen, Z., Gong, W., Wu, J., Yu, B., 2020b. Effects of urban forms on CO_2 emissions in China from a multi-perspective analysis. J. Environ. Manag. 262 (110300) https://doi.org/10.1016/j.jenvman.2020.110300.

Shi, K., Yu, B., Zhou, Y., Chen, Y., Yang, C., Chen, Z., Wu, J., 2019. Spatiotemporal variations of CO_2 emissions and their impact factors in China: a comparative analysis between the provincial and prefectural levels. Appl. Energy 233–234, 170–181. https://doi.org/10.1016/j.apenergy.2018.10.050.

Soliz, A., 2021. Divergent infrastructure: uncovering alternative pathways in urban velomobilities. J. Transport Geogr. 90, 2926–2926.

Son, C.H., Baek, J.I., Ban, Y.U., 2018. Structural impact relationships between urban development intensity characteristics and carbon dioxide emissions in Korea. Sustainability 10 (6). https://doi.org/10.3390/su10061838.

Stagakis, S., Chrysoulakis, N., Spyridakis, N., Feigenwinter, C., Vogt, R., 2019. Eddy Covariance measurements and source partitioning of CO_2 emissions in an urban environment: application for Heraklion. Greece. Atmos. Environ 201, 278–292. https://doi.org/10.1016/j.atmosenv.2019.01.009.

Su, K., Lee, C., 2021. Spatial dependence pattern of energy-related carbon emissions and spatial heterogeneity of influencing factors in China: based on ESDA-GTWR Model. Nat. Environ. Pollut. Technol. 20 (1), 29–38. https://doi.org/10.46488/NEPT.2021.v20i01.003.

Sun, H., Li, M., Xue, Y., 2019. Examining the factors influencing transport sector CO_2 emissions and their efficiency in central China. Sustainability 11 (17). https://doi.org/10.3390/su11174712.

Wang, J.F., Zhang, T.L., Fu, B.J., 2016. A measure of spatial stratified heterogeneity. Ecol. Indic 67, 250–256. https://doi.org/10.1016/j.ecolind.2016.02.052.

United Nations, 2014. 2014 Revision of the World Urbanization Prospects. Department of Economic and Social Affairs. https://population.un.org/wup/default.aspx.

Vittinghoff, E., Glidden, D.V., Shiboski, S.C., McCulloch, C.E., 2012. Regression methods in biostatistics: linear, logistic, survival, and repeated measures models. In: Second ed. Springer, New York.

Wang, S., Fang, C., Wang, Y., Huang, Y., Ma, H., 2015. Quantifying the relationship between urban development intensity and carbon dioxide emissions using a panel data analysis. Ecol. Indicat. 49, 121–131. https://doi.org/10.1016/j.ecolind.2014.10.004.

Wang, S., Liu, X., Zhou, C., Hu, J., Ou, J., 2017. Examining the impacts of socioeconomic factors, urban form, and transportation networks on CO_2 emissions in China's megacities. Appl. Energy 185, 189–200. https://doi.org/10.1016/j.apenergy.2016.10.052.

Wang, S., Zeng, J., Huang, Y., Shi, C., Zhan, P., 2018. The effects of urbanization on CO_2 emissions in the Pearl River Delta: a comprehensive assessment and panel data analysis. Appl. Energy 228, 1693–1706. https://doi.org/10.1016/j.apenergy.2018.06.155.

Wu, Y., Sharifi, A., Yang, P., Borjigin, H., Murakami, D., Yamagata, Y., 2018. Mapping building carbon emissions within local climate zones in Shanghai. Energy Proc. 152, 815–822. https://doi.org/10.1016/j.egypro.2018.09.195.

Xia, L., Zhang, Y., Sun, X., Li, J., 2017. Analyzing the spatial pattern of carbon metabolism and its response to change of urban form. Ecol. Model. 355, 105–115. https://doi.org/10.1016/j.ecolmodel.2017.03.002.

Xu, X., Ou, J., Liu, P., Liu, X., Zhang, H., 2021. Investigating the impacts of three-dimensional spatial structures on CO_2 emissions at the urban scale. Sci. Total Environ. 762 (143096) https://doi.org/10.1016/j.scitotenv.2020.143096.

Yang, W., Chen, B.Y., Cao, X., Li, T., Li, P., 2017. The spatial characteristics and influencing factors of modal accessibility gaps: a case study for Guangzhou, China. J. Transport Geogr. 60, 21–32. https://doi.org/10.1016/j.jtrangeo.2017.02.005.

Ye, H., He, X., Song, Y., Li, X., Zhang, G., Lin, T., Xiao, L., 2015. A sustainable urban form: the challenges of compactness from the viewpoint of energy consumption and carbon emission. Energy Build. 93, 90–98. https://doi.org/10.1016/j.enbuild.2015.02.011.

Zhang, H., Peng, J., Wang, R., Zhang, J., Yu, D., 2021. Spatial planning factors that influence CO_2 emissions: a systematic literature review. Urban Clim. 36 (100809) https://doi.org/10.1016/j.uclim.2021.100809.

Zhang, J., Xie, Y., Luan, B., Chen, X., 2015. Urban macro-level impact factors on direct CO_2 emissions of urban residents in China. Energy Build. 107, 131–143. https://doi.org/10.1016/j.enbuild.2015.08.011.

Zheng, B., Huo, H., Zhang, Q., Yao, Z.L., Wang, X.T., Yang, X.F., Liu, H., He, K.B., 2014. High-resolution mapping of vehicle emissions in China in 2008. Atmos. Chem. Phys. 14, 9787–9805. https://doi.org/10.5194/acp-14-9787-2014, 2014.

Zuo, S., Dai, S., Ren, Y., 2020. More fragmentized urban form more CO_2 emissions? A comprehensive relationship from the combination analysis across different scales. J. Clean. Prod. 244, 118659. https://doi.org/10.1016/j.jclepro.2019.118659.